Nanoscale

COMMUNICATION

View Article Online
View Journal | View Issue

Cite this: *Nanoscale*, 2014, **6**, 11637

Received 15th May 2014
Accepted 28th July 2014

DOI: 10.1039/c4nr02662d

www.rsc.org/nanoscale

Directed assembly of nanoparticles to isolated diatom valves using the non-wetting characteristics after pyrolysis†

A. Jantschke,[a] C. Fischer,[a] R. Hensel,[c] H.-G. Braun[b] and E. Brunner*[a]

A novel strategy for a directed nanoparticle coupling to isolated *Stephanopyxis turris* valves is presented. After pyrolysis, the valves exhibit incomplete wetting due to their characteristic T-shaped profiles as a prerequisite for a regioselective coupling reaction. A micromanipulation system allows for precise handling and their immobilization onto an adhesive substrate and manipulation into arrays.

Introduction

Diatoms[1] are an interesting and beautiful example of micro- and nanostructured materials occurring in nature. These unicellular, eukaryotic algae are found in almost all aquatic environments on earth and are well known for their intricately ornamented silica cell walls. With approximately 200 000 species, diatoms offer an enormous diversity of shapes and structures. Diatoms can have up to 100 million descendants within one month which makes them a cheap and renewable source of micro- and nanostructured silica materials.[1] Diatoms have attracted research interest due to their extraordinary material properties such as mechanical strength or remarkable elastic moduli[2–5] and they provide model organisms for studying biomineralization processes.[6,7] Their uniformly patterned diatom cell walls (valves) are assumed to be photonic crystal slab waveguides.[8,9]

Due to their special structure, *Coscinodiscus* valves can act as optical lenses.[10–12] Diatom biosilica of this genus exhibits wavelength-dependent transmission and reflection properties.[12–14] Light can be coupled into photonic crystal like modes. For example, the girdleband structures of *Coscinodiscus* were shown to act as optical waveguides for green-blue light.[8] Optical effects may be enhanced by surface modification or transformation reactions resulting in stronger refractive index contrasts. Gold replicas of *C. asteromphalus* exhibit an extraordinary optical transmission (EOT) for special IR wavelengths caused by surface plasmon effects.[15] A NIR photonic bandgap is observed for *Pinnularia* sp. frustules, which were decorated with magnetite nanoparticles.[16] The development of new surface modification methods is, therefore, essential for novel photonic applications.

Using diatom biosilica structures as a template material for nanoparticle assembly may offer exciting opportunities for emerging applications[15,17–20] in the fields of optics, (opto)electronics, photovoltaics, sensors, and catalysis. Combining the remarkable photonic/optical properties of nanoparticles and of the valves themselves may lead to prospective miniaturization of optical circuits or even to novel information transfer methods based on plasmons.[21–23]

In terms of fabrication, mimicking of the complex silica structures provided by diatom valves is difficult as well as time- and cost-intensive. Current research is, therefore, focused either on transforming diatom biosilica into other, non-silicon materials[24–30] or the surface modification by deposition methods,[31] *in situ* NP synthesis[32–35] or the attachment of prefabricated NPs.[36–39] Here, we present a novel strategy which allows the regioselective coupling of prefabricated nanoparticles to diatom valves by employing the non-wetting behavior of pyrolyzed diatom valves. The attached prefabricated nanoparticles exhibit uniform sizes and surface properties.

Wetting of solid surfaces is an important property[40] that is influenced by the surface morphology and chemistry. It can be adjusted by changing morphology and/or surface chemistry with respect to several applications such as self-cleaning,[41] drag reduction in flow,[42] anti-icing,[43] or anti-fogging.[44] Despite the fact that the materials properties and structural details of diatom valves are well-known, their wetting characteristics have not yet been studied.

[a]*TU Dresden, Fachrichtung Chemie und Lebensmittelchemie, Bioanalytische Chemie, 01062 Dresden, Germany. E-mail: eike.brunner@tu-dresden.de*

[b]*Max Bergmann Center of Biomaterials, Leibniz Institute of Polymer Research Dresden, 01069 Dresden, Germany*

[c]*INM – Leibniz Institute for New Materials, Campus D2 2, 66123 Saarbrücken, Germany*

† Electronic supplementary information (ESI) available: BET surface area, TG/DTA measurements, HIM images and a video of an array of six valves of *S. turris* in a wetting experiment as well as a 3D animation based on CLSM measurements. See DOI: 10.1039/c4nr02662d

The wetting behavior of a liquid droplet on an ideal (smooth, homogeneous, and rigid) solid surface can be determined by Young's equation.[45] However, the roughness of a surface significantly affects the macroscopic wetting behavior. Two models describing the different situations were developed: the Wenzel model[46] assumes that the liquid homogeneously wets the rough surface. In contrast, the Cassie–Baxter model[47] predicts that air remains entrapped underneath the liquid inside the grooves of the rough surfaces. That means, the liquid only wets the topmost parts of the asperities, a situation denoted as a Cassie state. A thermodynamically metastable Cassie state is usually achievable by means of a hydrophobic material (intrinsic contact angle higher than 90°) and an appropriately chosen roughness. However, the Cassie state is also feasible for a hydrophilic material (intrinsic contact angle lower than 90°) by the inhibition of liquid penetration into the grooves of the rough surface caused by special surface features with overhanging, *e.g.*, T-like structures. This effect was recently demonstrated for springtail skin.[48–50]

In the present work, we characterize the wetting characteristics of isolated valves extracted from *S. turris*. Several extraction and cleaning methods were tested and characterized concerning the remaining wettability of the valves. The obtained incomplete wetting behavior of pyrolyzed diatom valves was further utilized for regioselective functionalization by metal and semiconductor NPs using two different deposition strategies: a covalent coupling of nanoparticles and a layer-by-layer deposition using polyelectrolytes.

Results and discussion

The diatom species *Stephanopyxis turris* is a centric diatom with valve diameters of the order of 50 μm that allow handling by a micromanipulation system. The complex silica cell wall structure of *S. turris* with its characteristic dimensions is described in Fig. 1. The main feature of *S. turris* valves is a honeycomb-like structure with hexagonal chambers (areolae). A perforated layer with large holes (foramen) covers the areolae such that the cross-section of the silica cell wall exhibits T-like structure elements. Another silica layer showing a highly regular pore pattern covers the bottom of the areolae (sieve plate or cribrum).

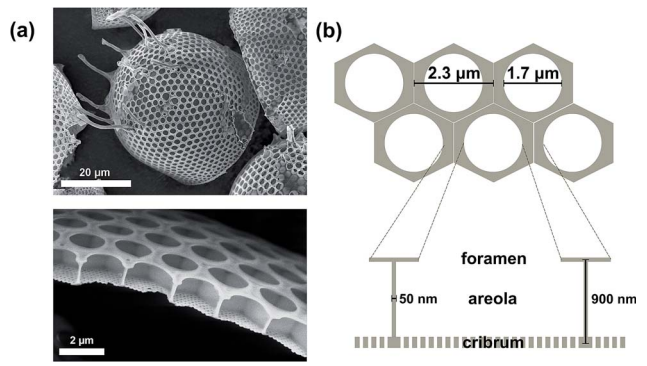

Fig. 1 Characteristic structure and dimensions of *S. turris* valves.

Note that the tubular extensions (processes) are connecting the cells into linear strands.

Diatom biosilica is a hybrid material which consists of amorphous silica and several organic compounds, *e.g.*, long-chain polyamines,[51–54] silaffins,[55–58] silacidins,[59,60] cingulins,[7] frustulins,[61] and polysaccharides.[62–66] These organic species are attached to or embedded into the inorganic silica phase. To investigate their influence on the wetting behavior of the siliceous valves, different extraction and pretreatment procedures were tested especially with respect to the remaining content of organic material. First, a common biosilica extraction method is performed by immersion of diatoms into a buffer solution containing EDTA and SDS.[67] Using this method, the remaining organic material—in the form of strongly silica-associated species—makes up about 10–15 wt% of the *S. turris* biosilica.[68,69] The content of organic material was reduced down to 1 wt% (Fig. S1 in the ESI†) by an oxidative treatment[70,71] using H_2O_2. Furthermore, we established a subsequent pyrolysis step at 500 °C under an argon atmosphere to remove the residual organics after EDTA/SDS-based extraction and H_2O_2-cleaning. The organic content could then be reduced down to 0.7 wt%.

To investigate the wetting behavior of the differently treated single diatom frustules, their precise and non-destructive positioning and immobilization onto a substrate was essential. This could be accomplished using a micromanipulation setup in combination with an optical microscope for *in situ* observations. Scheme 1 illustrates the basic steps of the diatom placement: a single valve was picked up from a slide covered with diatom biosilica powder using a thin cannula and subsequently transferred onto a sticky slide covered with an adhesive polymer. Using this procedure, arrangements of isolated cell walls (between 4 and 20) could be prepared, which were utilized for wetting experiments and nanoparticle coupling reactions.

Wetting characteristics of isolated diatom valves after different treatments

The wetting behavior of valves after several treatments was studied after complete immersion in aqueous media and observed *in situ* by optical microscopy (Fig. 2 and ESI, Movie M1†). As a control, hydrophobized valves were prepared by covering the valve surface with trimethylsilyl (TMS) moieties by hexamethyldisilazane (HMDS) coupling. During immersion, an air bubble remained inside the valve showing that the water could not immediately penetrate through the highly perforated diatom cell wall. Note that damaged or misplaced diatom shells were water-filled instantaneously. Water slowly penetrated into the valves after EDTA/SDS extraction, H_2O_2 treatment and calcination with progressing time. This was visible as a slow shrinkage of the entrapped air bubble inside the valves at the time scale of *ca.* 1 minute. In contrast, the pyrolyzed as well as hydrophobized (*i.e.*, HMDS-treated) samples remained free of water for at least 2 minutes.

That means a stable Cassie state without collapse of the air bubble inside the valve could be observed for the pyrolyzed and hydrophobized samples although all samples exhibited the same characteristic overhanging cross-sectional profiles. To

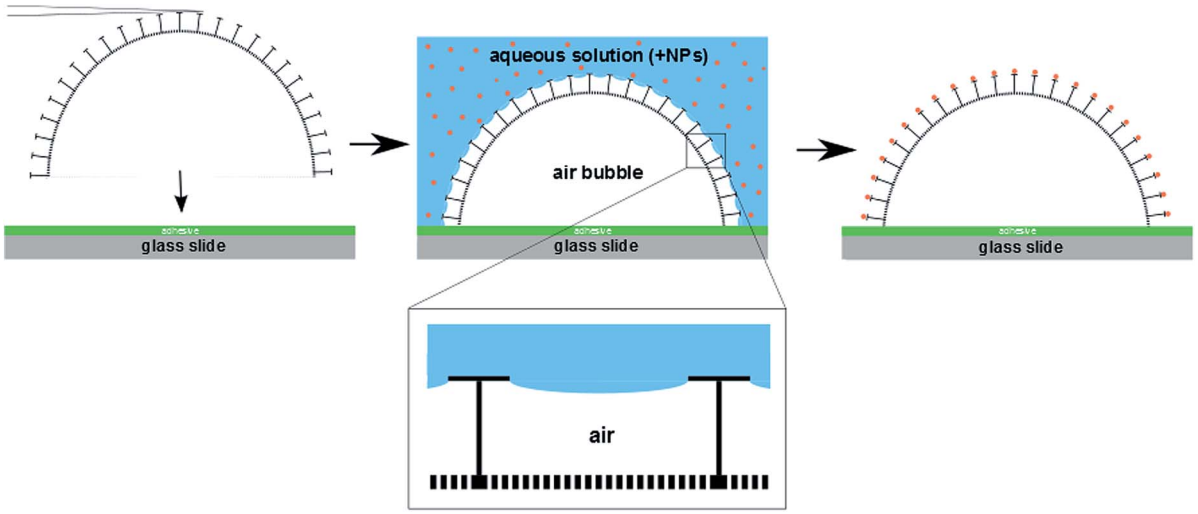

Scheme 1 Valve positioning and treatment using the micromanipulating system. From left to right: (i) a diatom valve is positioned on a glass slide using the cannula. The valves are embedded in an adhesive polymer. (ii) Nanoparticle solution is dropped on top of the valves and after a certain reaction time removed by rinsing with water. (iii) Nanoparticles remain on the wetted outer surface regions.

verify this result, we performed an additional air plasma cleaning step of the pyrolyzed valves. Plasma cleaning removes contaminants and generates a hydrophilic probe surface. As expected, the air bubble collapses again after 1 minute due to the enhanced surface hydrophilicity after plasma cleaning. A similar effect becomes obvious by comparing the effects of calcination and pyrolysis. Thermal treatment at identical temperatures in the presence (calcination) and absence (pyrolysis) of oxygen leads to significantly different results. The calcination process removes the organic material in the form of gaseous CO_2. In contrast, pyrolysis leaves a higher amount of carbon, probably in the form of graphitic species. This results in a less hydrophilic surface explaining the observed higher stability of the Cassie state.

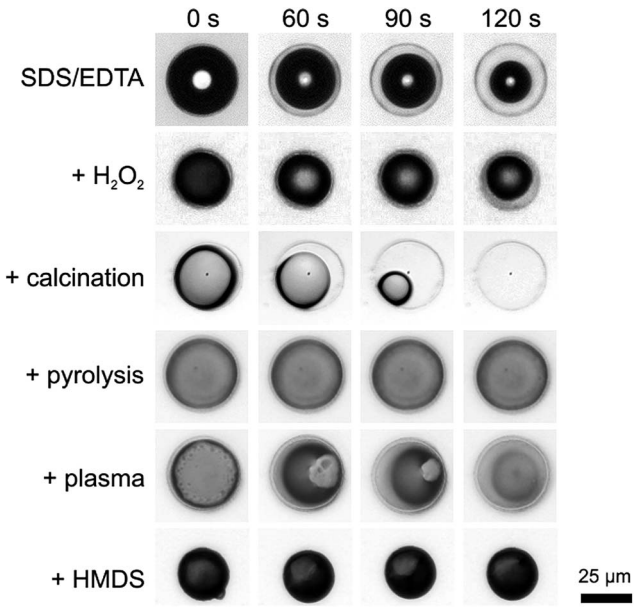

Fig. 2 Wetting behavior of *S. turris* valves as a function of time. First row: SDS/EDTA-treated valve slowly filling up with water (note: the air bubble inside the cell wall appears dark in the images, the white spot in the center of the cell wall is an artifact). Second row: the H_2O_2-treated sample shows a similar behaviour. The air bubble is stable for about 1 minute. Third row: calcination leads to an immediate collapse of the air bubble. Fourth row: the pyrolyzed valve shows the best results, the air bubble remains intact for at least 2 minutes. Fifth row: after additional air plasma cleaning (2 min), the air bubble collapses already after 1 minute. Sixth row: as hydrophilised reference sample, biosilica was treated with hexamethyldisilazane (HMDS). The air bubble then remained intact for at least 5 minutes.

We conclude that the characteristic surface structure of the valves in combination with the hydrophilicity—which is related to the presence of the organic material—determines the wetting behavior of the valves, *i.e.*, the long-term stability of the entrapped air bubble. Wetting of the valve interior is initially prevented by the overhanging, T-shaped cross-sectional structures of the diatom walls. Nevertheless, the water penetrates the pores with progressing time until the air bubble finally collapses, depending on the organic material content and state. We suggest that the organic material remaining after extraction and cleaning treatments enabled the penetration of water through the pores by creeping or intercalating along the organic phase into the valve.

To further investigate the influence of the pyrolysis process, we determined the BET surface area of the samples (Fig. S2 in the ESI†). H_2O_2-cleaned biosilica exhibits a BET surface area of about 50 $m^2\ g^{-1}$. After pyrolysis (500 °C) in an argon atmosphere, the surface area is reduced to 30 $m^2\ g^{-1}$.

We suppose that sintering and/or carbon deposition in pores are side effects of the pyrolysis process causing the decrease in surface area. To estimate the carbon content, thermogravimetric analysis (Fig. S3 in the ESI†) was performed in two stages: (i) heating up to 600 °C under an argon atmosphere with simultaneous mass spectrometry and (ii) heating from 600 °C to 800 °C under oxygen flow. During the heating, the adsorbed

water is first released. At stage (i), pyrolysis takes place. The mass spectrometric signals of $H_2O^{+\bullet}$ (18) and OH^+ (17) observed during the pyrolysis are indicative of alcohols or carboxylic acids. At stage (ii), the organic material/carbon of the samples was oxidized in an exothermic reaction resulting in gaseous CO_2. The pyrolysis reaction at stage (i) corresponds to the formation of intrinsically hydrophobic carbon (graphite, density = 2.26 g cm^{-3}). Assuming that this carbon forms a surface layer, the layer thickness would be circa 0.5 nm taking into account the measured BET surface. Plasma cleaning removes this carbon layer partly leading to enhanced water penetration into the valves. We, therefore, conclude that the pyrolytic removal of the organic material was accompanied by the formation of graphitic carbon deposits contributing to the long-term stability of the Cassie state.

The stability of the Cassie state over a reasonably long time up to several minutes is the necessary prerequisite for regioselective functionalization of single diatom valves. Due to the incomplete wetting behavior of the pyrolyzed diatom valves, the liquid is in contact with the T-shaped cross-sectional structures only (see Scheme 1). The surface of these wetted T-structures can be adjusted by various silica modification reactions, like aminosilane functionalization or polymer grafting.[72] Based on our previous work,[38] we chose to further utilize the incomplete wetting behaviour for regioselective functionalization with metal and semiconductor NPs using two different deposition strategies. The resulting materials were characterized by confocal laser scanning microscopy (CLSM) and backscatter scanning electron microscopy (BSE).

Directed assembly of nanoparticles to the pyrolyzed diatom valves

Toster *et al.* reported an *in situ* regiospecific synthesis of gold nanoparticles around the pores of diatoms[33] based on the dewetting of poly(vinylpyridine) (PVP). Thin films of this polymer were able to dewet reversibly during exposure to different pH environments and offered the possibility to control the regiospecific growth of gold NPs to the PVP domains. However, diatomite—the fossilized remnants of diatoms—were used in these experiments which exhibited only a single layered structure.

For the design of optically active three-dimensional NP arrays, diatom classes with multi-layer silica shells (cribrum or cribellum structures) like *Coscinodiscus* or *Stephanopyxis* are of particular interest. For this purpose, a novel strategy for the regioselective modification of multi-layered diatom valves is necessary. In contrast to the previously reported *in situ* preparation of NPs, we focused our present work to the attachment of pre-fabricated nanoparticles showing a narrow size distribution in combination with the obtained non-wetting behavior of the diatom valves after pyrolysis.

We applied two different approaches for the surface modification; "covalent" coupling[73] and a layer-by-layer approach.[74–78] For "covalent" coupling, the NPs were first coated with (3-aminopropyl)trimethoxysilane (APTMS). Subsequently, they were covalently linked to the biosilica by immersion of the valves into the aqueous NP suspension at room temperature.[73] Using this method, the NPs are coupled to the diatom biosilica after one immersion step only.

Several polyelectrolytes were used as "electrostatic coupling agents" in the second approach, the so-called layer-by-layer deposition technique. Negatively charged NPs could be assembled onto a positively charged polyelectrolyte which was first immobilized at the diatom valves. Polyallylamine hydrochloride (PAH) was used, which covered the negatively charged surface of the diatom cell walls after pyrolysis. To attach NPs to the surface of the diatom valve, two immersion steps were required: first into a PAH-containing solution and subsequently into the negatively charged NP suspension. This approach offered the opportunity to modify the diatom surface with PAH before positioning at the slide with the micromanipulation system and fixation. Deposition of NPs at the glass slide is thus prevented, *i.e.*, exclusively the diatom valves are NP-coated. This gives rise to a better signal-to-noise ratio in the CLSM measurements as shown in Fig. 3.

Both methods can be applied to couple different types of NPs to diatom valves. The layer-by-layer deposition can be repeated several times to obtain high surface coverage. For the characterization of the NP-coupled valves, confocal laser scanning microscopy (CLSM) and backscatter scanning electron microscopy (BSE) were used. For CLSM, 3.6 nm CdTe-NPs stabilized by thioglycolic acid (TGA) with an extinction maximum at 643 nm were coupled to *S. turris*. Citrate-stabilized Au-NPs with a diameter of 4 nm and an extinction maximum at about 505 to 506 nm were used for the detection by BSE and HIM.

CLSM images of pyrolyzed, CdTe-NP-coupled diatom valves are shown in Fig. 4. The characteristic structures of the *S. turris* silica are clearly visible at all focus levels (Fig. 4(a)). Using z-stacked fluorescence data, it was even possible to generate a 3D image of the diatom valve (see ESI, Movie M2†). While the perforated top layer with the large holes (foramen) showed a high fluorescence signal, the lower layer with the small holes (cribrum) did not show any significant fluorescence signal. This result indicated an efficient regioselective coupling of NPs only to the outermost layer of the hexagonal silica structures. As a

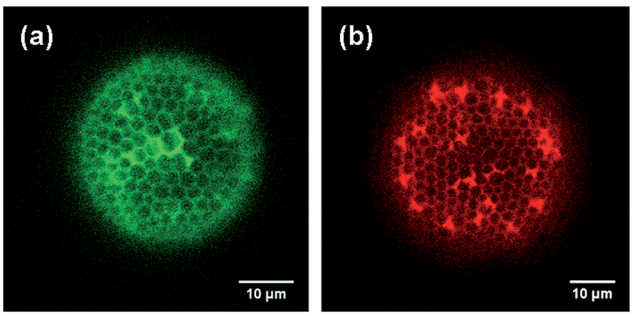

Fig. 3 Comparison of CLSM images of CdTe NPs regioselectively attached to a diatom valve using covalent coupling (a) and the layer-by-layer approach (b). Note that the color encoding can be chosen arbitrarily. Green symbolizes covalent coupling, red the layer-by-layer approach. Note that the tubular extensions (*cf.* Fig. 1(a)) are visible as strongly fluorescent spots especially in (b).

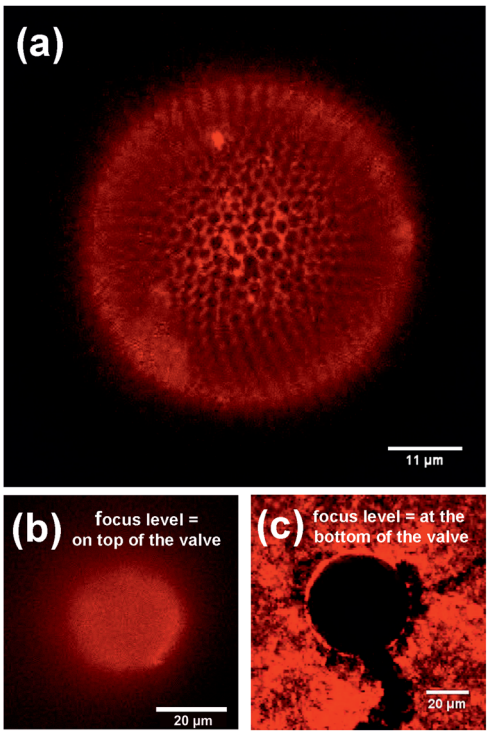

Fig. 4 CLSM images of CdTe NPs regioselectively attached to a diatom valve (a). Images of a reference sample are shown which is non-selectively covered with NPs after air-drying of the NP-containing coupling reagent solution (b and c).

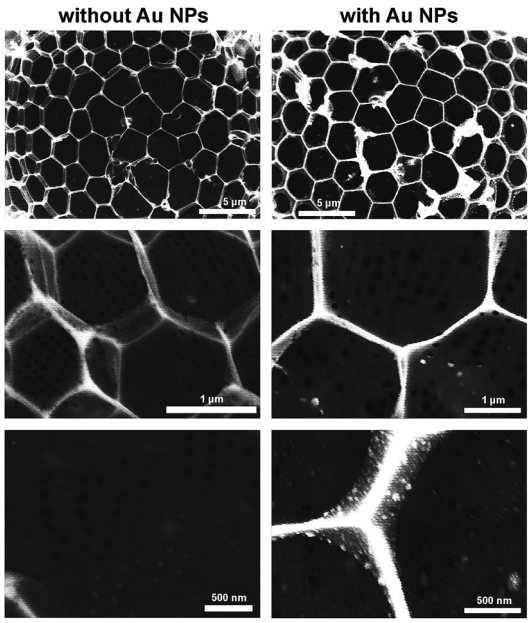

Fig. 5 Backscatter electron microscopic images of pyrolyzed biosilica without (left) and with (right) regioselectively assembled Au-NPs (layer-by-layer method). The images were taken under identical conditions. Note the tendency of noble metal nanoparticles to aggregate.

control, the CdTe-NP solution was left to evaporate on the valve (Fig. 4(b) and (c)). The micrograph in Fig. 4(c) clearly demonstrates that the liquid did not penetrate into the interior of the diatom shell, even during the evaporation of the solvent, such that only the valve and the surrounding substrate were covered by the remaining NPs. The outer surface of the valve is continuously covered by NPs, *i.e.*, no regioselectivity is observed in this control.

To further investigate the spatial distribution of the NPs inside the diatom cell walls, backscatter electron microscopy was utilized. The number of backscattered electrons and, hence, the brightness depend on the atomic number *Z*. In order to ensure the comparability of the obtained results, all pictures were recorded with the same brightness and contrast settings. It is obvious from all backscatter electron microscopic images (Fig. 5) that the brightness of the structures is enhanced by the deposition of Au NPs. The NPs are almost exclusively found on the characteristic T-structures and cannot be observed on the cribrum.

High resolution topological information of the cribrum structure can be obtained by helium ion microscopy (HIM),[79] a recently developed scanning microscopy technique based on SEM technology. Briefly, the method generates He ions at a very low pressure which originate from collisions with electrons emitted from an ultrasharp tip. The focused highly monochromatic ion beam (spot size down to 0.25 nm) guarantees a lateral resolution much higher than field emission SEM. The

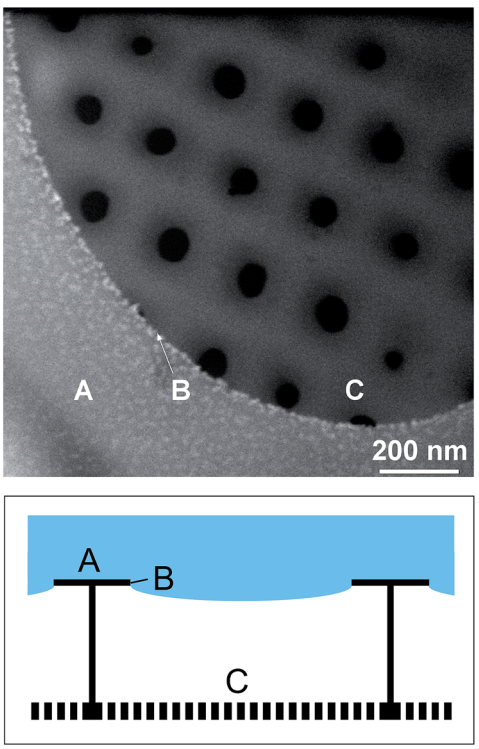

Fig. 6 High resolution He-ion microscopic image (top) of pyrolyzed biosilica with regioselectively assembled Au-NPs (layer-by-layer method). Corresponding wetting scheme (bottom): wetted outer surface (A), the three phase contact line (B) and cribrum (C).

scattering behaviour of He ions favours enhanced material contrast. Although the imaging is performed using particles of 30 keV, sample charging by positive ions can be compensated by electron injection from a flood gun. Consequently, surface coating of the samples is not necessary.

The high resolution He-ion microscopy image in Fig. 6 clearly demonstrates nanoparticle deposition exclusively on the outer surface. The cribrum structure is completely free of nanoparticles. Position B indicates the three phase contact line of the liquid–solid–gas interface. As a control we have studied a reference sample without attached nanoparticles (ESI, Fig. S4.1†). As expected only clean silica surfaces are observed. Furthermore, the effect of defect silica structures is also demonstrated (ESI, Fig. S4.2†). A mechanical crack results in less selective NP coupling, *i.e.*, penetration of the coupling solution into the areola.

In summary, all characterization methods confirmed the regioselective decoration of the cell wall with NPs.

Conclusions

Taken together, the inhibited penetration of aqueous solutions into the interior of diatom valves was successfully utilized for regioselective modification by NP coupling. To obtain a long-term stable Cassie state, the content of organic material associated with the biosilica had to be reduced by extraction, cleaning, and pyrolysis. As a proof of principle, we demonstrated that the developed approach is applicable for different nanoparticle coupling techniques and types of NPs. This regioselective NP coupling technique is also applicable to pre-assembled diatom arrays which may be produced either by micromanipulation or other approaches such as the floating assembly[80] or inkjet printing.[81]

Experimental

Cultivation of diatoms

Stephanopyxis turris was isolated from the North Sea in June 2004 by Prof. Manfred Sumper (Regensburg). Cultivation is performed in a 20 liter polycarbonate vessel (Nalgene) with artificial seawater (ASW) medium prepared according to the protocol of the North East Pacific Culture Collection.[82] Growth of *S. turris* in 20 liters of sterile filtered (0.2 lm, Kleenpak) ASW medium takes about 3 to 4 weeks. A RUMED 1301 light thermostat (18 °C, 12 h/12 h day/night cycle, *ca.* 1000 lux) provides constant growing conditions. The pH rise occurring during growth is readjusted using 2.5 M HCl. Cells are harvested by consecutive filtration of the culture medium with an 11 μm nylon mesh (Stockhausen Sieb- und Filtererzeugnisse) and subsequent centrifugation (Heraeus biofuge primo, swinging bucket rotor, 1000 rcf). The resulting pellets were frozen with liquid nitrogen and stored at −20 °C.

Cell wall extraction

Cell wall extraction follows the protocol described by Kröger *et al.*[67] In order to remove physically bound organic material from the cell walls, a buffer containing EDTA (0.1 M) and SDS (2%) at pH 8 is used. The harvested cells are suspended in 20 ml buffer solution and heated to 95 °C for 10 minutes. This treatment is repeated three times. Finally, the biosilica is washed at least three times with Milli-Q water. In all steps, the biosilica is separated from the supernatants *via* centrifugation (Heraeus biofuge primo, swinging bucket rotor, 1000 rcf, 10 min). After extraction, the samples are freeze dried or directly used for further purification steps.

To further remove the organic material from the biosilica, an oxidative treatment with H_2O_2 is performed. The biosilica is suspended in 20 ml of hydrogen peroxide (∼30%) and heated to 95 °C for 1 hour. This treatment is repeated three times and the biosilica is washed at least three times with Milli-Q water. In all steps, the biosilica is separated from the supernatants *via* centrifugation (1000 rcf). The biosilica is subsequently freeze-dried.

Further removal of the organic material is accomplished by pyrolysis at 500 °C for 3 hours under continuous Argon-flow. Calcination was performed using the same conditions but under an air atmosphere.

Hydrophobization of diatoms is achieved by TMS-functionalization. The biosilica is suspended in a solution of hexamethyldisilazane (Fluka) in toluene (5 wt%) and the solution is stirred overnight. Finally, the biosilica is washed at least three times with toluene and subsequently freeze-dried.

Micromanipulation system

For exact placement of single diatom valves onto slides, an Olympus IX70 microscope equipped with two micromanipulators (Eppendorf 5171) is used.

Slides are cleaned with chloroform and ethanol in an ultrasonic bath for 10 minutes. Activation of silanol groups is achieved by treatment with air plasma for 2 minutes. A thin layer of Acronal 500 D (Kremer Pigmente GmbH & Co. KG) is deposited *via* spin coating to prepare an adhesive layer. With the help of the thin cannula which is part of the micromanipulation system, single cell walls are picked from an untreated slide and transferred to the sticky slide. In a typical experiment, 4 to 20 cell walls are placed into an array. The slides are finally heated up to the transition temperature of the polyacrylate (120 °C, 10 min) which results in a tight sealing of cell walls onto the slides.

Nanoparticle coupling reagents

Covalent coupling. For covalent coupling the pH value of the TGA-stabilized CdTe-NPs (for NP synthesis, see below) is adjusted to a value between 6 and 7. 500 μl of the NP solution are mixed with 100 μl PBS buffer (pH 7.4) and subsequently with 500 μl of a mixture of *N*-hydroxysuccinimide (NHS, 50 mM, 98%, Aldrich) and *N*-(3-dimethylaminopropyl)-*N*′-ethylcarbodiimide hydrochloride (EDC, 10 mM, Sigma-Aldrich). Finally, 20 μl of (3-aminopropyl)trimethoxysilane (APS, 97%, 1 : 200 in H_2O, Alfa Aesar) are added. The solution is freshly prepared for each assembly.

For gold-NP attachment, 1 ml APS (1 mM) were added to 5 ml citrate-stabilized Au-NP solution and mixed for 15 min.

Layer-by-layer. For the layer-by-layer deposition technique, as-synthesized NPs were used (see below).

Nanoparticle assembly

Covalent coupling. The freshly prepared solution is dropped onto the diatom valves placed on the slide. Variable reaction and repetition times were used as given in the text. After reaction, the slide is rinsed with Milli-Q water and left to dry on air or in a moderate nitrogen flow. This procedure can be repeated several times to obtain good coverage.

Layer-by-layer. For the layer by layer assembly, two possible preparation types exist: (i) the diatom valves can be treated with the polyelectrolyte polyallylamine hydrochloride (PAH) before positioning on the slide. (ii) Alternatively, they can first be positioned on the slide and afterwards be treated with the polyelectrolyte and NPs as described for the covalent coupling above.

(i) Diatom biosilica (~2 mg) is suspended in 2 ml of the polyelectrolyte solution (1.5 ml; 1% PAH in 0.1 M sodium chloride). The solution is mixed for 15 min and washed at least three times with Milli-Q water by centrifugation (Heraeus biofuge primo, swinging bucket rotor, 700 rcf, 7 min). After positioning on a slide with the micromanipulator, a drop of the NP solution is added and left for 2 minutes followed by washing with Milli-Q water.

(ii) The positioned diatoms are covered with a drop of the polyelectrolyte solution (1.5 ml; 1% PAH in 0.1 M sodium chloride). After a reaction time of 2 minutes the slide is rinsed with Milli-Q water and dried in nitrogen flow and the NP solution is dropped onto the valves for a further 2 minutes. The slide is then washed again. The procedure can be repeated many times to gain good coverage.

Nanoparticle syntheses

The standard synthesis is performed as follows: 0.985 g (2.35 mmol) of $Cd(ClO_4)_2 \cdot 6H_2O$ (Alfa Aesar) are dissolved in 125 ml of water, and an appropriate amount of the thiol stabilizer is added under stirring, followed by pH-adjustment by dropwise addition of a 1 M solution of NaOH. The solution is placed in a three-necked flask fitted with a septum and valves and is deaerated by N_2 bubbling for 30 min. Under stirring, H_2Te gas is passed through the solution together with a slow nitrogen flow. CdTe-nanocrystal (NC) precursors are formed at this stage (reaction 1); formation and growth of NCs (reaction 2) proceed upon refluxing at 100 °C under open-air conditions with an attached condenser.

Gold nanoparticles with an extinction maximum at about 505 to 506 nm are prepared at room temperature. In a typical synthesis, 2.9 ml of a 0.2% solution of gold(III) chloride trihydrate (Sigma-Aldrich, 99.9+ %) in deionized water (Milli-Q) are added into a flask together with 500 ml deionized water. 11.6 ml of a 1% solution of sodium citrate in deionized water are added. After 30 seconds 5.8 ml of a freshly prepared ice-cold solution consisting of 0.085 g sodium borohydride and 0.5 g sodium citrate in 50 ml deionized water are injected quickly.

Nanoparticle solutions were used for assembly experiments as prepared without further purification or concentration.

Measurements

SEM. SEM/BSE images were acquired on a ZEISS DSM 982 GEMINI field emission scanning electron microscope. The arrays were put on an aluminium sample holder on top of a carbon tab. For the SEM images an acceleration voltage of 4 kV was applied. BSE images were taken with an acceleration voltage of 15 kV.

HIM. HIM measurements were performed using an ultra-high vacuum (UHV) Orion Plus helium ion microscope from Zeiss. All images were recorded with 30 keV accelerating voltage at a working distance of 8.3 mm.

BET. Nitrogen physisorption (−196 °C) measurements were performed on a Quantachrome Autosorb 1C apparatus. Specific surface areas were calculated using the BET equation in the P/P_0 range from 0.05 to 0.20.

CLSM. CLSM images were recorded on a Zeiss LSM 510 Meta instrument at the Biotechnology Centre, TU Dresden.

Elemental analysis. Elemental analysis was performed using a Eurovektor Hekatech EA-3000 Elemental Analyzer.

Acknowledgements

Thanks are due to Professor Alexander Eychmüller for helpful discussions. Excellent experimental assistance in SEM measurements by Ellen Kern and Susanne Goldberg is gratefully acknowledged. Furthermore, we thank Erdinc Sezgin for CLSM and Martin Oschatz for BET surface area measurements. Special thanks are due to Dr Gregor Hlawacek, HZDR, for measurements at the helium ion microscope. Financial support from the Deutsche Forschungsgemeinschaft (SPP 1569, grants no. Br 1278/24-1, 25-2) is gratefully acknowledged.

Notes and references

1 F. E. Round, R. M. Crawford and D. G. Mann, *The Diatoms: the Biology and Morphology of the Genera*, Cambridge University Press, 1990.
2 N. Almqvist, Y. Delamo, B. L. Smith, N. H. Thomson, Å. Bartholdson, R. Lal, M. Brzezinski and P. K. Hansma, *J. Microsc.*, 2001, **202**, 518–532, DOI: 10.1046/j.1365-2818.2001.00887.x.
3 C. E. Hamm, R. Merkel, O. Springer, P. Jurkojc, C. Maier, K. Prechtel and V. Smetacek, *Nature*, 2003, **421**, 841–843.
4 G. Subhash, S. Yao, B. Bellinger and M. R. Gretz, *J. Nanosci. Nanotechnol.*, 2005, **5**, 50–56.
5 D. Losic, K. Short, J. G. Mitchell, R. Lal and N. H. Voelcker, *Langmuir*, 2007, **23**, 5014–5021, DOI: 10.1021/la062666y.
6 M. Sumper and E. Brunner, *ChemBioChem*, 2008, **9**, 1187–1194, DOI: 10.1002/cbic.200700764.
7 A. Scheffel, N. Poulsen, S. Shian and N. Kröger, *Proc. Natl. Acad. Sci. U. S. A.*, 2011, **108**, 3175–3180, DOI: 10.1073/pnas.1012842108.

8 T. Fuhrmann, S. Landwehr, M. El Rharbi-Kucki and M. Sumper, *Appl. Phys. B: Lasers Opt.*, 2004, **78**, 257–260, DOI: 10.1007/s00340-004-1419-4.
9 L. De Stefano, P. Maddalena, L. Moretti, I. Rea, I. Rendina, E. De Tommasi, V. Mocella and M. De Stefano, *Superlattices Microstruct.*, 2009, **46**, 84–89, DOI: 10.1016/j.spmi.2008.10.031.
10 L. D. Stefano, I. Rea, I. Rendina, M. D. Stefano and L. Moretti, *Opt. Express*, 2007, **15**, 18082–18088, DOI: 10.1364/OE.15.018082.
11 E. D. Tommasi, I. Rea, V. Mocella, L. Moretti, M. D. Stefano, I. Rendina and L. D. Stefano, *Opt. Express*, 2010, **18**, 12203–12212, DOI: 10.1364/OE.18.012203.
12 K. Kieu, C. Li, Y. Fang, G. Cohoon, O. D. Herrera, M. Hildebrand, K. H. Sandhage and R. A. Norwood, *Opt. Express*, 2014, **22**, 15992–15999, DOI: 10.1364/OE.22.015992.
13 J. Noyes, M. Sumper and P. Vukusic, *J. Mater. Res.*, 2008, **23**, 3229–3235, DOI: 10.1557/JMR.2008.0381.
14 S. Yamanaka, R. Yano, H. Usami, N. Hayashida, M. Ohguchi, H. Takeda and K. Yoshino, *J. Appl. Phys.*, 2008, **103**, 074701, DOI: 10.1063/1.2903342.
15 Y. Fang, V. W. Chen, Y. Cai, J. D. Berrigan, S. R. Marder, J. W. Perry and K. H. Sandhage, *Adv. Funct. Mater.*, 2012, **22**, 2550–2559, DOI: 10.1002/adfm.201102715.
16 H. Li, B. Jiang, X. Yang, M. Eastman, Y. Liu, L. Wang, J. Campbell, L. Lampert, R. K. Wang, G. L. Rorrer and J. Jiao, *ACS Photonics*, 2014, **1**, 477–482, DOI: 10.1021/ph4001185.
17 M. Kucki and T. Fuhrmann-Lieker, *J. R. Soc., Interface*, 2012, **9**, 727–733, DOI: 10.1098/rsif.2011.0424.
18 W. Yang, P. J. Lopez and G. Rosengarten, *Analyst*, 2011, **136**, 42–53, DOI: 10.1039/C0AN00602E.
19 S. C. Davis, V. C. Sheppard, G. Begum, Y. Cai, Y. Fang, J. D. Berrigan, N. Kröger and K. H. Sandhage, *Adv. Funct. Mater.*, 2013, **23**, 4611–4620, DOI: 10.1002/adfm.201203758.
20 D. Zhang, Y. Wang, J. Cai, J. Pan, X. Jiang and Y. Jiang, *Chin. Sci. Bull.*, 2012, **57**, 3836–3849, DOI: 10.1007/s11434-012-5410-x.
21 M. Daniel and D. Astruc, *ChemInform*, 2004, **35**, 293–346, DOI: 10.1002/chin.200416213.
22 D. V. Talapin, J. Lee, M. V. Kovalenko and E. V. Shevchenko, *Chem. Rev.*, 2010, **110**, 389–458, DOI: 10.1021/cr900137k.
23 N. Gaponik, *J. Mater. Chem.*, 2010, **20**, 5174–5181.
24 K. Sandhage, M. Dickerson, P. Huseman, M. Caranna, J. Clifton, T. Bull, T. Heibel, W. Overton and M. Schoenwaelder, *Adv. Mater.*, 2002, **14**, 429–433, DOI: 10.1002/1521-4095.
25 R. R. Unocic, F. M. Zalar, P. M. Sarosi, Y. Cai and K. H. Sandhage, *Chem. Commun.*, 2004, 796–797, DOI: 10.1039/B400599F.
26 E. K. Payne, N. L. Rosi, C. Xue and C. A. Mirkin, *Angew. Chem., Int. Ed.*, 2005, **44**, 5064–5067, DOI: 10.1002/anie.200500988.
27 Z. Bao, M. R. Weatherspoon, S. Shian, Y. Cai, P. D. Graham, S. M. Allan, G. Ahmad, M. B. Dickerson, B. C. Church, Z. Kang, H. W. Abernathy III, C. J. Summers, M. Liu and K. H. Sandhage, *Nature*, 2007, **446**, 172–175.
28 Z. Bao, E. M. Ernst, S. Yoo and K. H. Sandhage, *Adv. Mater.*, 2009, **21**, 474–478.
29 C. Jeffryes, R. Solanki, Y. Rangineni, W. Wang, C. Chang and G. L. Rorrer, *Adv. Mater.*, 2008, **20**, 2633–2637, DOI: 10.1002/adma.200800292.
30 T. Qin, T. Gutu, J. Jiao, C. Chang and G. L. Rorrer, *ACS Nano*, 2008, **2**, 1296–1304, DOI: 10.1021/nn800114q.
31 D. Losic, J. G. Mitchell and N. H. Voelcker, *New J. Chem.*, 2006, **30**, 908–914, DOI: 10.1039/B600073H.
32 T. Gutu, D. K. Gale, C. Jeffryes, W. Wang, C.-hung Chang, G. L. Rorrer and J. Jiao, *J. Nanomater.*, 2009, 1–7, DOI: 10.1155/2009/860536.
33 J. Toster, K. S. Iyer, R. Burtovyy, S. S. O. Burgess, I. A. Luzinov and C. L. Raston, *J. Am. Chem. Soc.*, 2009, **131**, 8356–8357, DOI: 10.1021/ja901806y.
34 H. Zhou, T. Fan, X. Li, J. Ding, D. Zhang, X. Li and Y. Gao, *Eur. J. Inorg. Chem.*, 2009, 211–215, DOI: 10.1002/ejic.200800764.
35 J. Toster, Q. L. Zhou, N. M. Smith, K. S. Iyer, F. Rosei and C. L. Raston, *Green Chem.*, 2013, **15**, 2060–2063, DOI: 10.1039/C3GC40660A.
36 N. L. Rosi, C. S. Thaxton and C. A. Mirkin, *Angew. Chem., Int. Ed.*, 2004, **43**, 5500–5503, DOI: 10.1002/anie.200460905.
37 D. Losic, Y. Yu, M. S. Aw, S. Simovic, B. Thierry and J. Addai-Mensah, *Chem. Commun.*, 2010, **46**, 6323–6325, DOI: 10.1039/C0CC01305F.
38 A. Jantschke, A. K. Herrmann, V. Lesnyak, A. Eychmuller and E. Brunner, *Chem.–Asian J.*, 2012, **7**, 85–90, DOI: 10.1002/asia.201100563; 10.1002/asia.201100563.
39 F. Ren, J. Campbell, X. Wang, G. L. Rorrer and A. X. Wang, *Opt. Express*, 2013, **21**, 15308–15313, DOI: 10.1364/OE.21.015308.
40 K. L. Mittal, in *Contact Angle, Wettability and Adhesion*, VSP, Utrecht, The Netherlands, 1993, p. 519.
41 A. Solga, Z. Cerman, B. F. Striffler, M. Spaeth and W. Barthlott, *Bioinspiration Biomimetics*, 2007, **2**, S126.
42 J. Ou, B. Perot and J. P. Rothstein, *Phys. Fluids*, 2004, **16**, 4635–4643.
43 L. Cao, A. K. Jones, V. K. Sikka, J. Wu and D. Gao, *Langmuir*, 2009, **25**, 12444–12448, DOI: 10.1021/la902882b.
44 X. Gao, X. Yan, X. Yao, L. Xu, K. Zhang, J. Zhang, B. Yang and L. Jiang, *Adv. Mater.*, 2007, **19**, 2213–2217, DOI: 10.1002/adma.200601946.
45 T. Young, *Philos. Trans. R. Soc. London*, 1805, **95**, 65–87, DOI: 10.1098/rstl.1805.0005.
46 R. N. Wenzel, *Ind. Eng. Chem.*, 1936, **28**, 988–994, DOI: 10.1021/ie50320a024.
47 A. B. D. Cassie and S. Baxter, *Trans. Faraday Soc.*, 1944, **40**, 546–551, DOI: 10.1039/TF9444000546.
48 R. Hensel, R. Helbig, S. Aland, A. Voigt, C. Neinhuis and C. Werner, *NPG Asia Mater.*, 2013, **5**, e37.
49 R. Hensel, R. Helbig, S. Aland, H. Braun, A. Voigt, C. Neinhuis and C. Werner, *Langmuir*, 2013, **29**, 1100–1112, DOI: 10.1021/la304179b.
50 R. Hensel, A. Finn, R. Helbig, H. Braun, C. Neinhuis, W. Fischer and C. Werner, *Adv. Mater.*, 2014, **26**, 2029–2033, DOI: 10.1002/adma.201305408.

51 N. Kröger, R. Deutzmann, C. Bergsdorf and M. Sumper, *Proc. Natl. Acad. Sci. U. S. A.*, 2000, **97**, 14133–14138.
52 M. Sumper, S. Lorenz and E. Brunner, *Angew. Chem., Int. Ed.*, 2003, **42**, 5192–5195, DOI: 10.1002/anie.200352212.
53 M. Sumper, *Angew. Chem.*, 2004, **116**, 2301–2304, DOI: 10.1002/ange.200453804.
54 M. Sumper, E. Brunner and G. Lehmann, *FEBS Lett.*, 2005, **579**, 3765–3769, DOI: 10.1016/j.febslet.2005.06.001.
55 N. Kröger, R. Deutzmann and M. Sumper, *Science*, 1999, **286**, 1129–1132, DOI: 10.1126/science.286.5442.1129.
56 N. Kröger, S. Lorenz, E. Brunner and M. Sumper, *Science*, 2002, **298**, 584–586.
57 N. Poulsen, M. Sumper and N. Kröger, *Proc. Natl. Acad. Sci. U. S. A.*, 2003, **100**, 12075–12080, DOI: 10.1073/pnas.2035131100.
58 N. Poulsen and N. Kröger, *J. Biol. Chem.*, 2004, **279**, 42993–42999.
59 S. Wenzl, R. Hett, P. Richthammer and M. Sumper, *Angew. Chem., Int. Ed.*, 2008, **47**, 1729–1732, DOI: 10.1002/anie.200704994.
60 P. Richthammer, M. Börmel, E. Brunner and K. van Pée, *ChemBioChem*, 2011, **12**, 1362–1366, DOI: 10.1002/cbic.201000775.
61 N. Kröger, C. Bergsdorf and M. Sumper, *Eur. J. Biochem.*, 1996, **239**, 259–264.
62 R. E. Hecky, K. Mopper, P. Kilham and E. T. Degens, *Mar. Biol.*, 1973, **19**, 323–331, DOI: 10.1007/BF00348902.
63 B. E. Volcani, in *Cell Wall Formation in Diatoms: Morphogenesis and Biochemistry*, ed. T. Simpson and B. Volcani, Springer, New York 1981, pp. 157–200.
64 B. A. Wustman, M. R. Gretz and K. D. Hoagland, *Plant Physiol.*, 1997, **113**, 1059–1069.
65 M. J. McConville, R. Wetherbee and A. Bacic, *Protoplasma*, 1999, **206**, 188–200, DOI: 10.1007/BF01279266.
66 R. Hedrich, S. Machill and E. Brunner, *Carbohydr. Res.*, 2013, **365**, 52–60, DOI: 10.1016/j.carres.2012.11.001.
67 N. Kröger, C. Bergsdorf and M. Sumper, *EMBO J.*, 1994, **13**, 4676–4683.
68 E. Brunner and K. Lutz, in *Handbook of Biomineralization: Biomimetic and Bioinspired Chemistry*, ed. P. Behrens and E. Baeuerlein, Wiley-VCH, Weinheim, 2007, pp. 19–38.
69 C. Gröger, K. Lutz and E. Brunner, *Prog. Nucl. Magn. Reson. Spectrosc.*, 2009, **54**, 54–68.
70 S. A. Robinson, T. Williams and P. R. Bown, *Paleoceanography*, 2004, **19**, PA4024, DOI: 10.1029/2004PA001010.
71 B. Tesson, S. Masse, G. Laurent, J. Maquet, J. Livage, V. Martin-Jézéquel and T. Coradin, *Anal. Bioanal. Chem.*, 2008, **390**, 1889–1898, DOI: 10.1007/s00216-008-1908-0.
72 *Studies in Surface Science and Catalysis*, ed. E. F. Vansant, P. Van Der Voort and K. C. Vrancken, Elsevier, Amsterdam, 1995, vol. 93, pp. 3–556.
73 A. Shavel, N. Gaponik and A. Eychmüller, *ChemPhysChem*, 2005, **6**, 449–451, DOI: 10.1002/cphc.200400516.
74 G. Decher, *Science*, 1997, **277**, 1232–1237, DOI: 10.1126/science.277.5330.1232.
75 A. L. Rogach, D. S. Koktysh, M. Harrison and N. A. Kotov, *Chem. Mater.*, 2000, **12**, 1526–1528, DOI: 10.1021/cm0000649.
76 M. Gao and C. Lesser, *J. Appl. Phys.*, 2000, **87**, 2297–2302.
77 A. S. Susha, F. Caruso, A. L. Rogach, G. B. Sukhorukov, A. Kornowski, H. Möhwald, M. Giersig, A. Eychmüller and H. Weller, *Colloids Surf., A*, 2000, **163**, 39–44, DOI: 10.1016/S0927-7757(99)00428-8.
78 M. T. Crisp and N. A. Kotov, *Nano Lett.*, 2003, **3**, 173–177, DOI: 10.1021/nl025896f.
79 B. W. Ward, J. A. Notte and N. P. Economou, *J. Vac. Sci. Technol., B: Microelectron. Nanometer Struct.–Process., Meas., Phenom.*, 2006, **24**, 2871–2874, DOI: 10.1116/1.2357967.
80 Y. Wang, J. Pan, J. Cai and D. Zhang, *Biochem. Biophys. Res. Commun.*, 2012, **420**, 1–5, DOI: 10.1016/j.bbrc.2012.02.080.
81 W. Wang, T. Gutu, D. K. Gale, J. Jiao, G. L. Rorrer and C. Chang, *J. Am. Chem. Soc.*, 2009, **131**, 4178–4179, DOI: 10.1021/ja809079n.
82 P. J. Harrison, R. E. Waters and F. J. R. Taylor, *J. Phycol.*, 1980, **16**, 28–35, DOI: 10.1111/j.0022-3646.1980.00028.x.